Investigation of four-wave mixing in $Nd_xLa_{1-x}P_5O_{14}$

Jacek K. Tyminski and Richard C. Powell
Physics Department, Oklahoma State University, Stillwater, Oklahoma 74078

Walter K. Zwicker
Philips Laboratories, Briarcliff Manor, New York 10510
(Received 7 November 1983)

Four-wave mixing has been investigated in $Nd_xLa_{1-x}P_5O_{14}$ crystals as a function of temperature, laser excitation wavelength, and power. The results are interpreted in terms of scattering from a population grating, and the relative intensity of the scattered signal is investigated as well as the grating decay time. The power dependence of the scattered intensity is explained by a model involving interaction with a three-level system, and the properties of the grating decay are associated with the exciton dynamics of the ions in the excited state. Decay patterns characteristic of both incoherent and partially coherent exciton migration can be observed under different experimental conditions. Enhanced migration due to vibronic generation of phonons resonant with the metastable state splitting is also observed. The temperature dependence of the results shows a weak coupling between the excitons and the acoustic phonons of the host. Local heating effects are found to affect the ion-ion and ion-phonon interaction parameters and produce a thermal grating under certain experimental conditions.

I. INTRODUCTION

The dynamics of quasiparticle transport has long been a topic of fundamental interest in solid-state physics. Exciton migration among ions and molecules in highly concentrated crystals represents an important special case of this type of problem. Two of the most important questions which have been extensively addressed theoretically concern the distinction between coherent and incoherent motion[1-3] and spectral variations in migration efficiency.[4-6] It has proven to be quite difficult to find the appropriate experimental techniques and crystal systems to provide the data necessary to verify the theoretical predictions. We report here the results of using four-wave-mixing transient-grating spectroscopy to characterize the properties of $Nd_xLa_{1-x}P_5O_{14}$ crystals. This work demonstrates the powerful capabilities of this experimental technique for studying exciton-transport properties.

The technological potential of rare-earth pentaphosphates as minilasers has made it imperative to understand the basic optical properties of this class of materials.[7] An interesting dichotomy has developed in comparing the results obtained from site-selection laser spectroscopy techniques[8-10] which monitor spectral energy migration with results obtained from coherent transient techniques[11] which probe the spatial delocalization of the energy. The former indicate that weak spectral transfer occurs, while the latter show the excitation energy to be spatially delocalized. Our initial investigation using four-wave-mixing transient-grating spectroscopy produced results which demonstrated the existence of long-range exciton diffusion in $Nd_xLa_{1-x}P_5O_{14}$ crystals at room temperature.[12] In this paper we present the results of an investigation of the exciton-diffusion coefficient as a function of temperature, laser-pump power, and excitation wavelength. Also the variation of scattering efficiency as a function of pump power is reported. The results show that either incoherent or partially coherent exciton migration can occur depending on the initial excitation conditions. They also show the effects of local thermal heating on excitation-migration parameters.

The details of crystal growth and sample properties were described previously.[13] Figure 1 shows the pertinent energy levels and transitions for this study. The dye laser with Rodamine-6G pumps the Nd^{3+} ions in the region of the absorption band consisting of overlapping levels of the $^2G_{7/2}$ and $^4G_{5/2}$ manifolds. With high-energy vibronic excitation a photon is absorbed and a phonon is emitted. Rapid radiationless relaxation to the $^4F_{3/2}$ metastable

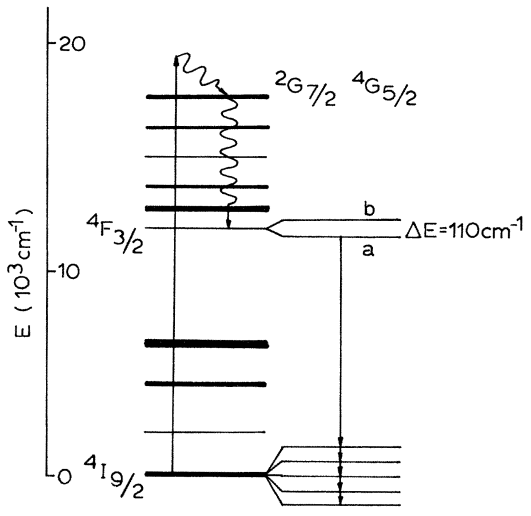

FIG. 1. Partial energy-level diagram for Nd^{3+} showing the excitation and emission transitions of interest to this work.

state then occurs. Fluorescence occurs from this level to the various components of the ^4I term. An extensive amount of work has been reported on the conventional optical spectroscopy of this material.[14–16] The energy in the metastable state can be transferred from one Nd^{3+} ion to another and this mobile excitation energy is treated as a Frenkel exciton.

II. FOUR-WAVE-MIXING TRANSIENT-GRATING SPECTROSCOPY

Figure 2 shows a block diagram of the experimental setup used for four-wave-mixing measurements. The output of an argon-ion laser-pumped tunable dye laser with Rhodamine-6G dye was split into three beams. By using a variable beam splitter and a variable neutral-density filter the power in each of these beams was controlled. Beams *a* and *b* are the pump beams. They are chopped and weakly focused inside the sample. Care was taken to ensure that the difference in their optical path lengths was less than the coherence length of the laser. The probe beam *p* enters the opposite side of the sample conjugate to pump beam *a* and the signal beam *s* exits the sample conjugate to pump beam *b*. Another beam splitter was used to send part of the signal beam to a photomultiplier tube. The time decay of the signal beam was processed by both a boxcar integrator and a signal averager before being displayed on a recorder. This double averaging technique gave excellent signal-to-noise—ratio results. The sample was mounted in a cryogenic refrigerator with a temperature controller which varied the temperature selectively between about 10 K and room temperature.

Four-wave mixing occurs through the third-order component of the susceptibility tensor. This can be related to local changes in the refractive index induced by the interacting laser pump beams. These changes can be produced by several physical mechanisms including thermal effects, photoconductive effects, and changes in electronic state populations. Each of these has specific characteristics different from the others, and thus it is generally possible to determine the dominant physical mechanism giving rise to the scattering for a specific system under given experimental conditions. There are two different approaches to describing this physical process.[17–19] One is through the use of Maxwell's equations and the susceptibility of the material to account for the nonlinear interaction of the laser beams in the solid. This method is generally used to determine the signal-generation efficiency as discussed in Sec. VI. The other approach is to treat the process as the scattering of the probe beam from a grating formed by the interfering pump beams.[19] This method is generally used to study the physical properties of the material which produce and destroy the grating. For the case of interest here, the scattering is due to a population grating. The interference pattern of the two pump beams is a sine wave. This results in the creation of a high density of Nd^{3+} ions in the metastable state in the peak regions of the sine wave and a low density of excited Nd^{3+} ions in the valley regions. Figure 3 schematically depicts this population grating.[20] The difference in the refractive index of the ions in the ground and excited states causes the scattering of the probe beam. The Bragg-diffraction condition is satisfied with the probe beam directed conjugate to one of the pump beams and scattering in the direction of the other pump beam.

The two primary experimental parameters to be measured are the scattering efficiency and the decay pattern of the signal beam when the pump beam is chopped off. The former information is of greatest interest in the practical application of four-wave mixing to optical data processing, while the latter information is useful in understanding the physical mechanisms which cause the destruction of the grating pattern. Both types of measurements are discussed in the following sections, but the latter is most important in using this technique to study exciton dynamics. As shown in Fig. 3, the grating is destroyed by the normal radiative and radiationless relaxation processes, and, in addition, by the migration of exci-

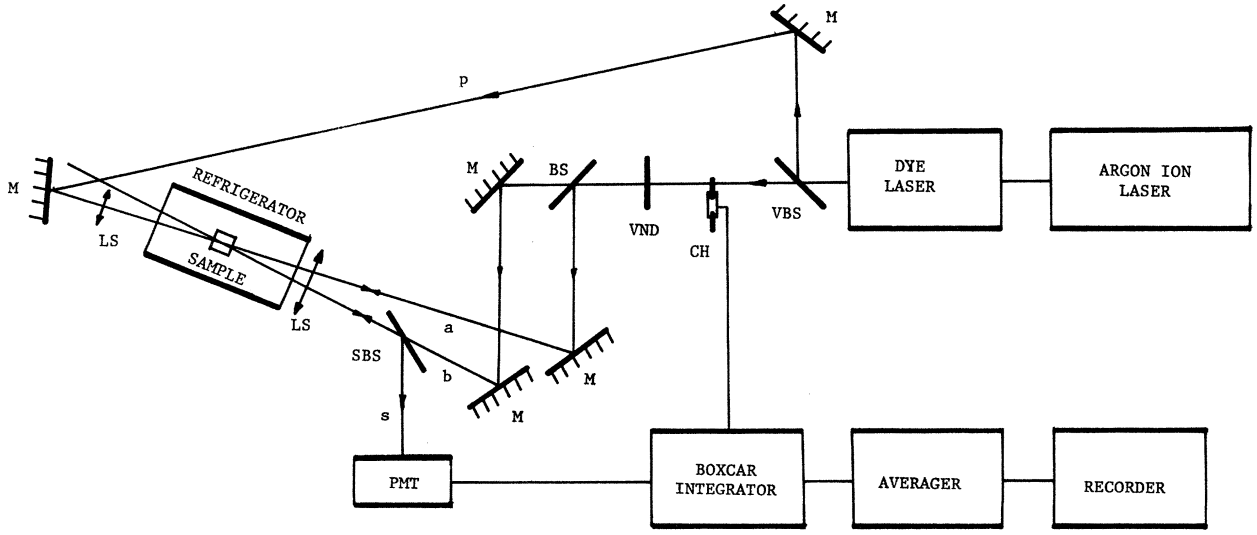

FIG. 2. Block diagram of the experimental apparatus. *M*, mirror; LS, lens; BS, VBS, and SBS, beam splitters; CH, chopper; PMT, photomultiplier tube.

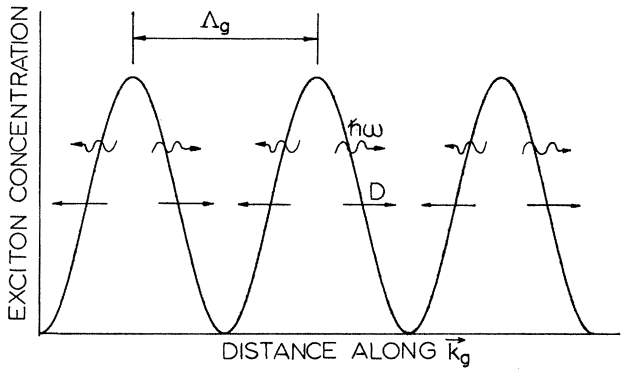

FIG. 3. Schematic representation of the population grating (Ref. 20). Λ is the grating wavelength.

tation energy from the peak to the valley regions of the population distribution. It is this last process of exciton migration which is of interest here, and the relationship between the properties of this migration and the measured experimental characteristics are discussed in the following section.

III. CHARACTERISTICS OF GRATING DECAY PATTERNS

Figure 4 shows the absorption spectrum of NdP_5O_{14} in the region of the laser wavelength at 77 K. This type of stoichiometric rare-earth material has high optical densities in the regions of peak absorption, and therefore the pump, probe, and signal beams are strongly depleted for this type of excitation. Strong beam depletion makes it difficult to perform four-wave-mixing experiments and to interpret the results. Therefore these experiments were performed by exciting into the high-energy wing of the absorption transition or by using Stokes vibronic excitation. Each point in the figure represents the results of determining the exciton-diffusion coefficients for $Nd_xLa_{1-x}P_5O_{14}$ samples with $x=1.0$ and 0.2 using transient-grating data as described below. These measurements were made at 12.5 K using weakly focused laser beams.

Figure 5 shows examples of the three different types of

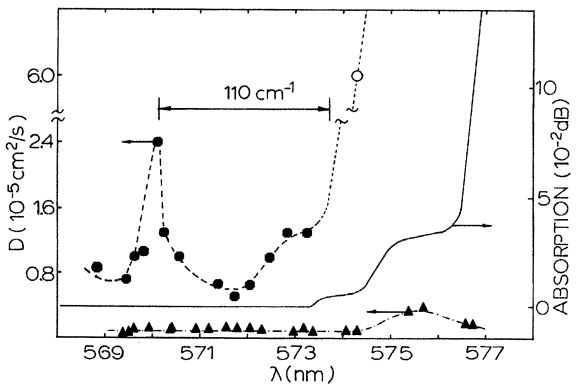

FIG. 4. Excitation wavelength dependence of the exciton-diffusion coefficient with respect to the absorption spectrum for $P_p=0.18$ W. Absorption spectrum taken at 77 K and values for D obtained at 12.5 K. ○ represents data for the $x=1.0$ sample and △ represents data for the $x=0.2$ sample.

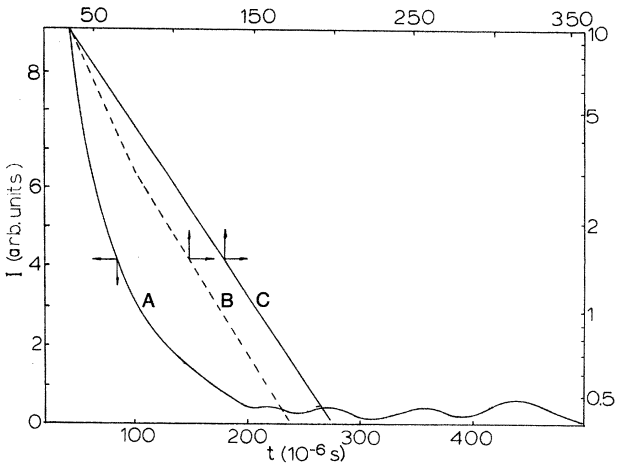

FIG. 5. Examples of signal decay patterns observed at 12.5 K at $\theta=10°$. *A*, $\lambda_{exc}=5745$ Å; $P_p=0.03$ W. *B*, $\lambda_{exc}=5745$ Å; $P_p=0.18$ W. *C*, $\lambda_{exc}=5724$ Å; $P_p=0.18$ W. $x=1.0$.

grating decay patterns that were observed for different types of experimental conditions. These traces show the excellent signal-to-noise ratio obtained with the dual-averaging technique. Under most conditions the single exponential decay is observed, which is consistent with results of previous work of this type.[12,20–24] This pattern is always observed for the $x=0.2$ sample. It is also always observed for the $x=1.0$ sample when vibronic excitation is used. However, for resonant excitation into the wing of the absorption band of the $x=1.0$ sample, the other two types of decay patterns can be observed. The oscillatory pattern was observed at low temperatures using total laser-pump powers of less than 30 mW. If the temperature is raised to about 100 K, the oscillatory pattern disappears and a single exponential pattern is observed. If the power is increased, the double exponential decay pattern is seen. The physical significance of these different types of grating decay patterns is discussed below.

Since the use of transient-grating techniques to study exciton migration is fairly recent, there has been little work done in developing and testing theoretical models for interpreting experimental results. Several different types of approaches to this problem have been employed. The two most useful formalisms for developing specific expressions describing population grating decay patterns are due to Fayer[20] and to Wong and Kenkre.[25] Fayer's results have been derived for the two limiting cases of purely incoherent and purely coherent exciton migration. In his formalism, the latter case is applicable for the initial experimental conditions of direct, resonant excitation into the exciton band leading to strongly delocalized states. The Wong and Kenkre approach has been developed for the general case of partially coherent exciton migration as well as the two limiting cases. The Fayer and the Wong and Kenkre results have been shown to be equivalent in the purely incoherent migration limit if the continuum approximation is made in both cases. However, the Fayer and the Wong and Kenkre formalisms lead to quite different results in the purely coherent migration limit. The reason is that the latter is based on a generalized master-

equation approach which requires the initial density matrix for the system to be diagonal. Physically, this restricts the applicability of the approach to initial experimental conditions of highly localized exciton states or complete phase randomness among the wave functions. This condition can be achieved experimentally by excitation into a higher-lying energy level followed by fast radiationless relaxation into the exciton band. As described in Sec. I, these are exactly the experimental conditions of the work described here. Therefore, the Wong-Kenkre theory is outlined below and their results are used to interpret the experimental data. The validity of this theory and other possible theoretical interpretations of the data are discussed further in Sec. VII.

Starting from a generalized master-equation approach, Wong and Kenkre[25] express the probability of finding an exciton on lattice site m at time t as $p_m(t)$ and its time evolution is described by

$$\frac{dP_m(t)}{dt}=\int_0^t dt'\left[\sum_n V_{m,n}(t-t')P_n(t') - V_{n,m}(t-t')P_m(t')\right]-P_m(t)/\tau\ . \quad (1)$$

Here τ is the exciton lifetime and $V_{m,n}(t)$ gives the rate of energy transfer from the mth to the nth site. This latter parameter is called the "memory function" since it reflects the degree of coherence influencing the energy-migration process. This function has been computed using a one-dimensional model with a time-independent, nearest-neighbor ion-ion—interaction matrix element j and a single, time-independent, randomized parameter α describing the exciton interaction with the phonon bath,[24]

$$V_{n,m}(t)=2j^2e^{-\alpha t}\{[J^2_{m-n+1}(2jt)+J^2_{m-n-1}(2jt)+2J_{m-n+1}(2jt)J_{m-n-1}(2jt)] - \{2J^2_{m-n}(2jt)+J_{m-n}(2jt)[J_{m-n+2}(2jt)+J_{m-n-2}(2jt)]\}\}\ , \quad (2)$$

where $J_1(x)$ is the Bessel function of the first kind and ith order. Substituting Eq. (2) into Eq. (1) and using Laplace-transform techniques gives[25]

$$I_s(t)=I_s(0)e^{-2t/\tau}\left[1-e^{-\alpha t}4j\sin(k_gd/2)\int_0^t du\,J_1(4ju\sin(k_gd/2))e^{\alpha(t^2-u^2)^{1/2}}\right]\ , \quad (3)$$

where d is the lattice constant in the grating direction.

This expression describes the time decay of the grating signal intensity in the presence of partially coherent exciton migration within the limitations of the model. Simpler expressions can be obtained from Eq. (3) for the limiting cases of purely coherent or purely incoherent exciton migration. The latter is the most important case since it is most commonly observed experimentally. The limiting conditions for this case are $\alpha\to\infty$ as j^2/α remains constant. The expression for the time dependence of the scattered-beam intensity becomes[25]

$$I_s(t)=I_s(0)\exp\{-2t[4F\sin^2(k_gd/2)+1/\tau]\} =I_s(0)e^{-Kt}\ , \quad (4)$$

where F is the transfer rate given by $F=2j^2/\alpha$, and

$$K=2[4F\sin^2(k_gd/2)+1/\tau]\ . \quad (5)$$

In the continuum approximation which usually applies, the exciton motion is considered to be diffusive with the diffusion coefficient given by

$$D=Fd^2=2j^2d^2/\alpha\ , \quad (6)$$

and so the decay rate in this case reduces to

$$K=2(k_g^2D+1/\tau)\ . \quad (7)$$

For the case of greater than nearest-neighbor ion-ion interaction, $F/2\alpha\to 0$, and Eq. (1) reduces to yield an exponential decay pattern

$$I_s(t)=I_s(0)\exp(-2t\{[\alpha^2+16j^2\sin^2(k_gd/2)]^{1/2}+\alpha+1/\tau\})=I_s(0)e^{-Kt}\ , \quad (8)$$

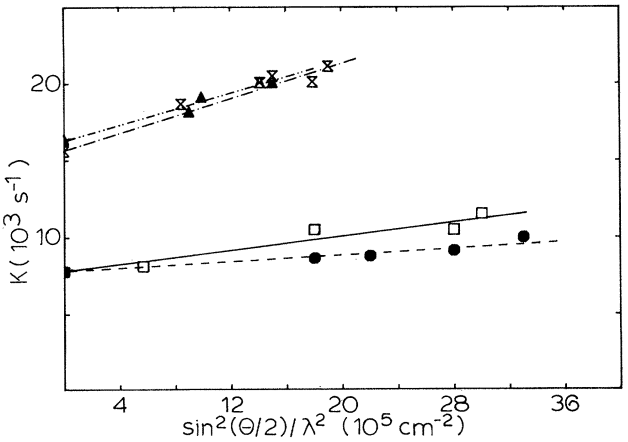

FIG. 6. Dependence of signal decay rate on crossing angle. ▲ and ⧖ are for $x=1.0$ with $\lambda_{exc}=5699$ Å where the former corresponds to $T=23$ K and the latter to 300 K. □ and ■ are for $x=0.2$ with $\lambda_{exc}=5749$ Å where the former corresponds to $T=28$ K and the latter to $T=300$ K.

TABLE I. Exciton-diffusion coefficient in $Nd_xLa_{1-x}P_5O_{14}$ crystals.

Excitation condition ($T=12.5$ K, $P_p=0.18$ W)	D (10^{-5} cm^{2}s^{-1}) $x=0.2$	$x=1.0$
Vibronic	0.1	0.8
Enhanced vibronic	0.1	2.4
Direct	0.4	6.0[a]

[a]Obtained from Eq. (6) with the short-time value of j and low value of α found from fitting the data obtained using a pump power of 0.03 W.

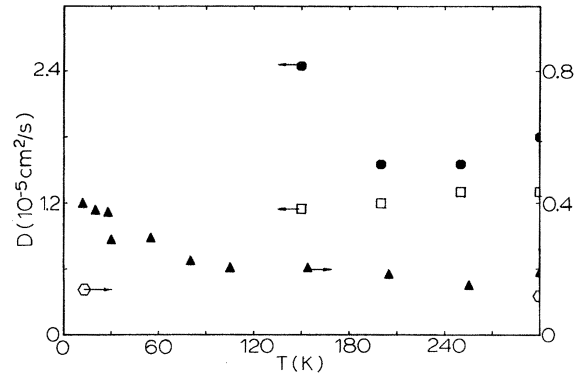

FIG. 7. Temperature dependence of the exciton diffusion coefficient for incoherent motion. ● and □ are for $x=1.0$, $\lambda_{exc}=5746$ Å, with laser-pump powers of 0.18 and 0.03 W, respectively. △ and ○ are for $x=0.2$, $\lambda_{exc}=5749$ Å, with laser-pump powers of 0.18 and 0.03 W, respectively.

where

$$K=2\{[\alpha^2+16j^2\sin^2(k_g d/2)]^{1/2}-\alpha+1/\tau\}\ . \quad (9)$$

In the following work we use Eq. (3) in fitting the data to determine the microscopic interaction parameters j and α. Then D is determined from Eq. (6) as a phenomenological parameter to characterize the macroscopic exciton migration. It must be emphasized that, in general, only the microscopic parameters have real physical meaning, whereas the parameter D only has an exact physical meaning within the limiting conditions discussed in deriving Eq. (6), and in other cases it should only be considered as a parameter used for comparative purposes to characterize the mobility of the excitons. An oscillatory grating decay pattern is predicted by Eq. (3), although an exact fit to the experimentally observed shape is not possible due to the limitations of the theoretical model as discussed in the following sections. The double exponential decay pattern shown in Fig. 5 cannot be theoretically described with a simple grating decay expression and is attributed to scattering from two types of gratings.

Figure 6 shows examples of results obtained by plotting the measured signal decay rate versus the crossing angle of the pump beams under the conditions giving single exponential decays. For each set of measurements the results vary as $\sin^2(\theta/2)$, and are extrapolated to independently measured values of $2/\tau$, as predicted by the simplified form of Eq. (3) given in Eq. (7). The diffusion coefficients found from fitting these data are listed in Table I. Their variations with excitation wavelength, temperature, and pump power are shown in Figs. 4, 7, and 8, respectively.

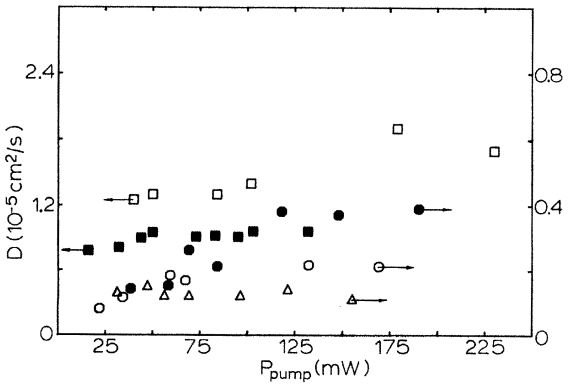

FIG. 8. Pump-power dependence of the exciton-diffusion coefficient for incoherent motion. ● is for $x=0.2$, $T=12.5$ K, and $\lambda_{exc}=5756$ Å. ○ is for $x=0.2$, $T=300$ K, and $\lambda_{exc}=5718$ Å. △ is for $x=0.2$, $T=300$ K, and $\lambda_{exc}=5749$ Å. □ is for $x=1.0$, $T=300$ K, and $\lambda_{exc}=5743$ Å. ■ is for $x=1.0$, $T=300$ K, and $\lambda_{exc}=5688$ Å.

IV. CHARACTERISTICS OF THE EXCITON-DIFFUSION COEFFICIENT

Figure 4 shows three interesting features in the dependence of D on excitation wavelength. First, for direct excitation into the absorption-band edge of the $x=1.0$ sample, nonexponential decay patterns are observed. This may be associated with partially coherent exciton migration and is discussed in the next section. The other two features are the enhancement of D after direct excitation of the $x=0.2$ sample and after vibronic excitation 110 cm^{-1} above the absorption-band edge for the $x=1.0$ sample. These effects can be attributed to enhancement of the ion-ion—interaction processes giving rise to incoherent exciton migration. In the latter case, this enhancement is associated with the creation of phonons of energy of 110 cm^{-1} in the vibronic excitation process. As seen in Fig. 1, this is the same energy as the crystal-field splitting of the $^4F_{3/2}$ metastable level, and thus the generation of 110-cm^{-1} phonons will cause an increase in the population of excited ions in the upper component of this manifold. The verification of this nonequilibrium population distribution is given by the emission spectra shown in Fig. 9. As the excitation wavelength is scanned into the region of vibronic enhancement increased emission from the upper level (b) of the metastable state can be distinctly seen. It is known from the absorption spectrum[14] that the transition between the b level and the ground state has a higher oscillator strength than the transition between the lower level (a) and the ground state.

For both cases of interest here (direct excitation of the $x=0.2$ sample and vibronic excitation of the $x=1.0$ sample), the assumptions leading to Eq. (6) are valid, and thus this expression can be used for the diffusion coefficient where j contains the matrix element for the interaction, $\alpha^{-1}=t_s$ is the exciton scattering time, and d is the lattice spacing. The matrix element depends on the oscillator strengths and the spectral overlaps of the transitions involved in the interaction. The scattering time has different properties depending on the mechanism limiting the exciton mean free path.[27,28] Thus the diffusion coefficient will increase with an increase in the oscillator strengths of the transitions involved in the energy transfer. The lack of increase in D in the 110-cm^{-1} phonon vibronic excitation region for the $x=0.2$ sample may be due to two reasons. The first is the generation of fewer phonons in the more lightly doped sample. The second is

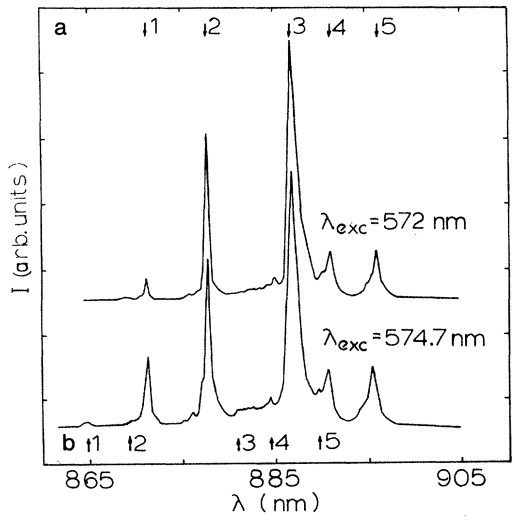

FIG. 9. Fluorescence emission of the $x=1.0$ sample at 12.5 K and a pump power of 0.18 W for two different excitation wavelengths.

the greater distance between Nd^{3+} ions which reduces the number of ions available for absorbing the 110-cm^{-1} phonons.

The increase in D in the region of direct excitation for the $x=0.2$ sample can be explained through the properties of site selection. The excitation transitions are inhomogeneously broadened due to random perturbations in the local crystal-field sites of the Nd^{3+} ions. The narrow-line laser excitation selectively excites the subset of ions having transitions in resonance with the excitation wavelength. As the laser is scanned toward the center of a transition, the concentration of ions in the resonant subset increases. This results in an increase in D because of the increase in the density of lattice sites involved in the exciton migration. For the particular case of interest here, there is a significant amount of structure within the absorption band associated with the overlap of several different discrete transitions. This structure is partially reflected in the variation of D with excitation wavelength as seen in Fig. 4.

Figure 7 shows the variation of D with temperature for an excitation wavelength just on the edge of the resonant absorption region and different laser powers. For low laser power, the value of D for the $x=0.2$ sample remains constant as temperature is lowered from room temperature to 12.5 K, while for the $x=1.0$ sample D is constant between room temperature and about 100 K, below which nonexponential decay patterns are observed. At high laser powers the room-temperature values of D are approximately the same as those obtained with lower powers, but a significant increase in D occurs at lower temperatures. As shown in Fig. 7, D increases continuously as temperature is lowered to 12.5 K, where it reaches a value which is approximately equal to that obtained with lower powers exciting in the peak region of resonant excitation shown in Fig. 4. The $x=1.0$ sample again exhibits nonexponential behavior below about 100 K.

There are several different types of physical process which can affect the temperature dependence of the diffusion coefficient. With reference to Eq. (9), these processes can be separated into two categories: those that change the group velocity v_g of the excitons, and those that alter the scattering time of the excitons. The fact that D is independent of temperature for low-pump-power conditions implies that the exciton-phonon scattering rate which contributes to t_s must be independent of temperature. For this to be true there must be weak coupling between the excitons and acoustical phonons which are present at low temperatures.[28] Strong scattering may occur from optical phonons, but at the temperatures of interest in this study, which range from slightly above to well below the Debye temperature, too few phonons of this type will be available for this to be an effective mechanism for limiting the exciton mean free path. Thus the major mechanism for exciton scattering must be lattice defects and boundaries which give a temperature-independent t_s. This implies that the parameter α from Eq. (3) in this case is dominated by exciton-defect interactions instead of exciton-phonon interactions. Therefore the origin of the observed temperature dependence at high powers must be due to processes affecting v_g. These cannot be intrinsic changes in parameters such as transition oscillator strengths and spectral overlaps since they do not occur with low excitation power. The most probable explanation appears to be a power broadening combined with the site-selection characteristics of laser excitation. At low temperatures the laser excitation is just on the edge of the resonant transition and the low value of D associated with the low concentration of the subset of ions excited. As power is increased this subset is saturated and ions in other subsets having Lorentzian wings overlapping the laser-excitation area become excited. This results in power broadening of the excitation spectrum so that subsets having higher concentrations of ions take place in the exciton-migration process. Activating these higher concentration subsets creates an increase in D similar to that observed when the laser excitation is scanned closer to the center of the resonant transition. As the temperature is raised, the spectral lines shift to lower energies so that the laser-excitation wavelength employed is no longer on the edge of the absorption transition, but rather is in the vibronic sideband area. In this case, saturation and power broadening is less effective and there is a decrease in the enhancement of D. Thus the observed temperature dependence of D for the $x=0.2$ sample at high laser powers is essentially associated with the temperature shift of the spectral line out of resonance with the laser excitation wavelength. The same may be true for the $x=1.0$ sample, but it is difficult to tell since the region of nonexponential decay occurs as D begins to vary strongly with T.

Figure 8 shows the change in D with pump power. For the majority of the experimental conditions investigated D did not vary with pump power. However, as shown in the figure, for the $x=0.2$ sample at 12.5 K with excitation in the area of the resonant transition, the value of D increases from its normal low value to its resonantly enhanced value as power is increased. Coupled with the

characteristics described above, this can again be attributed to a power-broadening effect.

V. CHARACTERISTICS OF EXCITON MIGRATION AFTER DIRECT EXCITATION

Next, we consider the results obtained on the $x=1.0$ sample at low temperatures for direct excitation into the absorption band. For low-laser-pump powers the oscillatory decay pattern shown in Fig. 5 is observed. The source of these oscillations is unknown and may be associated with several different types of physical processes. One possibility is the destruction of the grating through partially coherent exciton migration. In order to test this possibility, the results are analyzed in terms of a partially coherent exciton-migration model as discussed below. Oscillatory patterns of the grating decay are predicted by Eq. (3) from the model developed by Wong and Kenkre[25] for certain values of the parameters j and α. However, it was not possible to obtain a close fit to the decay patterns observed experimentally using Eq. (3) for two reasons. First, the frequency of the observed oscillations decreases with time, whereas the predicted value is a constant given by $4j\sin(k_g d/2)$. Second, the magnitudes of the oscillation peaks increase with time before damping out, instead of showing a uniform exponential decrease with time as theoretically predicted. These variations are shown graphically in Fig. 10. Both quantities exhibit a similar exponential variation with time.

An important physical process which can affect these results is local heating. As the excited Nd^{3+} ions relax radiationlessly to the metastable state, phonons are given off which produce a thermal grating pattern which follows the population grating. This local heating can produce three effects. The first is the variation of the ion-ion—interaction parameter j. The magnitude of j can be enhanced both by thermal broadening of the interaction transitions and by thermally populating higher crystal-field levels with stronger interaction properties. This enhancement of j should decrease with time as the phonons diffuse away from the locally heated region. This is confirmed by the results in Fig. 10 which show the oscillation frequency to decrease exponentially with the same decay time as the thermal grating, as discussed below.

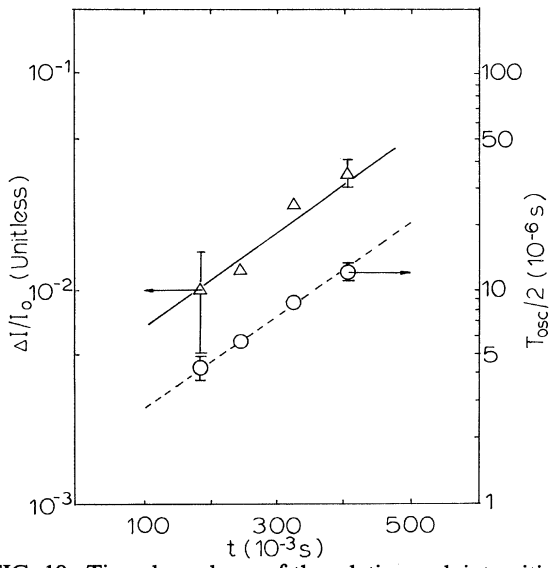

FIG. 10. Time dependence of the relative peak intensities and half-periods of the signal oscillations for $x=1.0$, $T=12.5$ K, $P_p=0.03$ W, and $\lambda_{exc}=5745$ Å. T_{osc} is the period of the oscillations.

The second possible effect of local heating is the modulation of the exciton scattering rate α. As discussed in the preceding section, acoustic phonons do not appear to be effective in scattering the excitons so any variation of α due to local heating would occur only if optical phonons are generated in the radiationless relaxation process. If this occurs, α would decrease with time as the optical phonons diffuse away from the locally heated area. According to Eq. (3) this change in α would decrease the rate of decay of the grating, but would not cause the peak magnitudes of the oscillations to increase with time. The latter may be associated with the decrease in j with time, which can be seen from Eq. (3) to cause an increase in signal intensity. Although it is tempting to interpret the results in this way, because of the similar time-dependent changes in the magnitude and frequency of the oscillations as shown in Fig. 10, there is no way to rule out the presence of more complex interference effects similar to those observed in coherent transient experiments.[29]

The third possible effect of local heating is probe-beam scattering from the thermal grating due to thermally induced changes in the refractive index. There is no evidence of contributions to the detected signal beam due to this effect at low-laser-pump powers where the oscillatory decay patterns are observed. However, at high pump powers the oscillations disappear and are replaced by a double exponential decay pattern. This can be attributed to simultaneous scattering of the probe beam from the thermal and population gratings. The slower decay rate is consistent with those extracted from the observed single exponential decay patterns of population gratings. Scattering from the thermal grating obscures the observation of any coherent oscillations which may be present. The decay pattern of the thermal grating is given by[30]

$$I_s(t)=I_s(0)e^{-2K_T t}, \tag{10}$$

where

$$I_s(0)=\tfrac{1}{4}I_p T_\lambda\left[\frac{2\pi d'}{\lambda}\frac{dn}{dt}\hat{T}\right]^2$$

and

$$K_T=16\pi^2\sin^2(\theta/2)D_T/\lambda^2 . \tag{11}$$

Here, $\hat{T}$ is the spatial temperature amplitude, D_T is the thermal diffusion coefficient, d' is the sample thickness, and T_λ is the transmission. The thermal properties of neodymium pentaphosphate crystals[31] predict a value of $D_T \lesssim 1\times10^{-2}$ cm^2 s^{-1}, which is consistent with the rough estimate of $D_T=3\times10^{-3}$ cm^2 s^{-1} obtained from the leading part of the double exponential decay.

Despite the complexities discussed above, it is possible to obtain numerical values for j from the observed frequencies of the oscillations and for α from fitting the initial decay of the signal shape. This gives a value of

$j=1.2\times10^7\ s^{-1}$ at short times and a much smaller value at long times, as seen in Fig. 10. Unfortunately, Eq. (3) is much less sensitive to the parameter α, and so the best fit to the experimental data can be obtained with any value of α between 10^4 and $3\times10^6\ s^{-1}$. By using the experimentally obtained values of j and α in Eq. (6), an estimate for the diffusion coefficient for partially coherent exciton motion can be obtained. This analysis, with the short-time value for j and the smallest value in the range of α, is the origin of the point plotted in the direct excitation region in Fig. 4 for the $x=1.0$ sample and the value of D listed in Table I. Note that this value of D is much greater than the values obtained for vibronic excitation, but it decreases significantly for long-time values of j or higher values in the range of α. The fact that partially coherent exciton migration was not observed for the $x=0.2$ sample implies the need for a high concentration of active ions to produce this type of motion. This can be attributed to the increase in the separation of Nd^{3+} ions which decreases the ion-ion—interaction rate.

VI. POWER DEPENDENCE OF SCATTERING EFFICIENCY

Another experimental measurement of interest is the power dependence of the scattering efficiency. Although this does not contain specific information concerning exciton dynamics, it does provide additional information concerning the characteristics of the four-wave-mixing interaction in the material. This type of information is especially useful in the application of this technique to areas such as optical data processing or phase conjugation. The experimental beam geometry used for these types of applications is different from the geometry used for studying exciton dynamics,[12,19,32–35] and this leads to different mathematical expressions for the scattering efficiency. The detailed outline of the mathematical development of the expression for scattering efficiency is given in Ref. 12. An extension of this development is presented below, in which some of the simplifying assumptions made previously are no longer used. In addition, in previous work the mechanism of field coupling is modeled by analyzing the response of a two-level system to the perturbations of the electric fields, whereas in the treatment outlined below an attempt is made to better model the true multilevel nature of the material by treating the susceptibility as the linear combination of the susceptibilities of two two-level systems, which has been suggested previously.[23]

The polarization of the medium is given by $P(E)=\epsilon_0\chi(E)E$, where ϵ_0 is the dielectric constant of free space and $\chi(E)$ is the dielectric susceptibility. The electric field in the medium can be separated into two parts, $E=E_0+\Delta E$, where the first part represents the contribution due to the two strong pump beams, while ΔE is the contribution due to the two weak probe and signal beams. The susceptibility of the multilevel system is approximated by

$$\chi=\frac{R}{R+1}\chi_1+\frac{1}{R+1}\chi_2\ , \tag{12}$$

where χ_1 is the susceptibility of the system with the ions in the ground state and χ_2 is the susceptibility of the system with the ions in the metastable state. $R=n_1/n_2$ where n_1 is the number of ions in the ground state and n_2 is the number of ions in the metastable state. Expanding the polarization to first order in $\Delta E/E_0$ gives

$$P(E_0+\Delta E)=\epsilon_0 e^{i\omega t}\sum_{i=1,2}R_i\chi_{0i}(E_0)\times\left[E_0+\Delta E-\frac{E_0\,\Delta E+|E_0|^2\Delta E}{I_{si}+|E_0|^2}\right], \tag{13}$$

where $R_1=R/(R+1)$, $R_2=1/(R+1)$, and

$$\chi_{0i}(E_0)=\frac{-2\alpha_{0i}}{k}\frac{I_{si}(i+\delta_i)(1+\delta_i^2)}{I_{si}+|E_0|^2}\ . \tag{14}$$

Here, the $i=1,2$ subscripts refer to the ions in ground and metastable states, respectively. α_0 is the line-center small-signal field-attenuation coefficient, δ_i is the detuning parameter, and I_{s0} is the saturation intensity.

The key approximations used in deriving the expression for the four-wave-mixing signal intensity are $\Delta E\ll E_0$, that the pump and probe beams are undepleted in traveling through the medium (parametric approximation), and the slowly varying envelope approximation.[12] By using these approximations and solving the wave equation in the medium, expressions can be obtained for the magnitudes of the electric field components at different positions along the direction of propagation. The square of these amplitudes gives the beam intensities. The quantity of greatest interest is the scattering efficiency defined as the ratio of the signal-beam intensity as it leaves the sample to the probe-beam intensity as it leaves the sample in the absence of pump beams. The general expression for this is quite complicated[18] and it is usually more convenient to simplify the expression by making appropriate assumptions. For interpreting data on the power dependence of the scattering efficiency, the least restrictive assumption[12] to make is that the crossing angle of the pump beams is sufficiently large that the amplitudes of the pump and signal fields do not change appreciably over the distance $\lambda_{os}=\lambda/(1-\cos\theta)$. This approximation holds for the angles used in the experiments described here. The resulting expression for scattering efficiency is

$$\eta=\left|\frac{\rho}{\zeta}\right|^2\frac{\exp(\Psi_{E_0})}{(\cos^{-1}\theta-1)^2}\{\exp(-2\zeta_R L)+\exp(-2\zeta_R L\cos^{-1}\theta)-2\exp[-\zeta_R L(1+\cos^{-1}\theta)]\cos[\zeta_I L(1-\cos^{-1}\theta)]\}\ , \tag{15}$$

where

$$\left|\frac{\rho}{\zeta}\right| = \frac{\sum_{j=1,2}\left[\sum_{i=1,2} F_{j,i}\frac{R_i\alpha_{0i}}{(1+\delta_i^2)I_{si}}\frac{(I_2I_4)^{1/2}[1+(I_2+I_4)/I_{si}]}{\{[1+(I_2+I_4)/I_{si}]^2-4I_2I_4/I_{si}^2\}^{3/2}}\right]^2}{\sum_{j=3,4}\left[\sum_{i=1,2} F_{j,i}\frac{R_i\alpha_{0i}}{1+\delta_i^2}\frac{[1+(I_2+I_4)/I_{si}]^2-2I_2I_4/I_{si}^2}{\{[1+(I_2+I_4)/I_{si}]^2-4I_2I_4/I_{si}^2\}^{3/2}}\right]^2} . \tag{16}$$

Here

$$F_{1,i}=\cos\Delta-\delta_i\sin\Delta\ ,\quad F_{3,i}=1\ ,$$
$$F_{2,i}=\sin\Delta-\delta_i\cos\Delta\ ,\quad F_{4,i}=\delta_i\ , \tag{17}$$
$$\Psi_{E_0}=(2L/\cos\theta)\sum_{i=1,2} R_i\alpha_{0i}/(1-\delta_i^2)\ .$$

Under more restrictive simplifying assumptions this expression reduces to the one obtained previously.[12] Although it is rather cumbersome to work with such a complicated equation in fitting experimental data, any further assumptions mask the results of some of the physical processes underlying the mechanisms of four-wave mixing in a multilevel medium. Figures 11 and 12 show the results of measuring scattering efficiency versus laser-pump power for both samples at room temperature with the excitation wavelength in the direct-transition spectral region. Measurements were made in two different ranges of power densities by changing the focused-beam cross-section area in the sample. The results change significantly for the two different measurement conditions, indicating that scattering efficiency is sensitive to power density as well as total pump power. It is immediately obvious that the results do not obey a simple quadratic dependence as predicted by a simple two-level–system model.[23] Instead, the curves are almost s-shaped with the curvature being more enhanced for the $x=1.0$ sample and being greater for lower power densities.

The solid lines in the figures represent the best fits to the data using Eq. (15) and treating R, δ_i, α_i, I_{0i}, and Δ (with $i=1,2$) as adjustable parameters. This was done on a Digital Equipment Corporation LSI-11 computer using a multiple-parameter, nonlinear-regression, least-squares-fitting routine. Although with a complex expression such as Eq. (15) involving eight adjustable parameters it should be possible to generate a variety of different curve shapes, it turns out in this case that to obtain any better fits to the data than those shown in the figure requires unphysical values for one or more of the fitting parameters. Table II lists the values of these parameters used to obtain the fittings shown in the figures. The fitting is good for the $x=0.2$ sample with high-power-density conditions, but for the low-power-density conditions it does not predict a curvature as strong as that observed in the experimental data. For the $x=1.0$ sample the fits are reasonably good for both power-density conditions in the regions of low total power, but significant disagreement between theory and experiment occurs in the high-total-power region.

Although there is no way to obtain exact values for the parameters in Table II from independent measurements, the values obtained from the fitting procedure are physically reasonable. It is interesting to note that for both samples the value of R required to obtain the best fit to the data is significantly greater in the high-power-density case compared to the low-power-density case. This would be expected if the multilevel model proposed here is valid. The fact that there is some discrepancy between theory and experiment shows that there are other physical processes occurring which are not taken into account in the model used here. One possible effect that might be important is beam depletion in the sample. This would be more important in the highly concentrated material, which is consistent with the poorer fit between theory and experiment obtained in the $x=1.0$ sample compared to the $x=0.2$ sample. Another improvement of the model

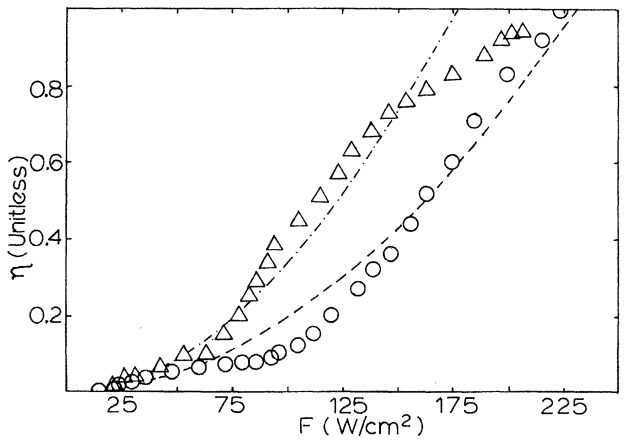

FIG. 11. Variation of scattering efficiency with pump-beam power at low-flux levels at $T=300$ K and a crossing angle of 10°. △ is for $x=1.0$ and $\lambda_{exc}=5145$ Å. ○ is for $x=0.2$ and $\lambda_{exc}=5750$ Å. See text for explanation of theoretical lines.

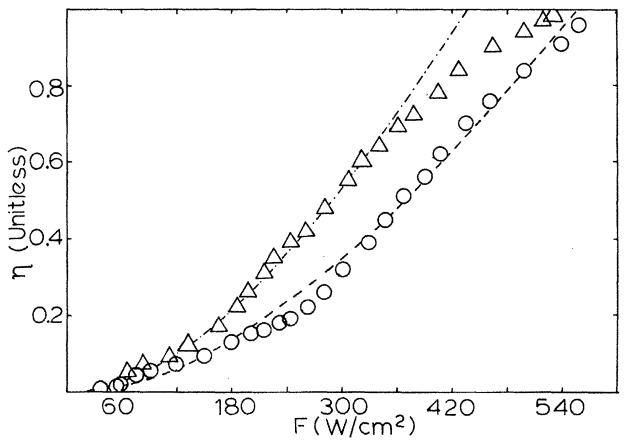

FIG. 12. Variation of scattering efficiency with pump-beam power at high-flux levels at $T=300$ K and a crossing angle of 10°. △ is for $x=1.0$ and $\lambda_{exc}=5750$ Å. ○ is for $x=0.2$ and $\lambda_{exc}=5750$ Å.

TABLE II. Scattering efficiency parameters at $T=300$ K and $\theta=10°$.

Parameters	High flux		Low flux	
	$x=1.0$	$x=0.2$	$x=1.0$	$x=0.2$
λ_x (nm)	575	575	514.5	575
R	1.0	1.0	0.01	0.01
δ_1	4.5	4.9	7.2	5.3
δ_2	0.1	0.1	0.1	0.1
α_1 (cm^{-1})	50	10	50	10
α_2 (cm^{-1})	45	9	45	9
I_{01} (W/cm^2)	4.0×10^3	4.0×10^3	3.9×10^3	4.0×10^3
I_{02} (W/cm^2)	5.0×10^3	5.0×10^3	5.0×10^3	5.0×10^3
Δ	6.0×10^{-11}	1.0×10^{-6}	6.0×10^{-7}	2.0×10^{-5}

would be to use expressions for Gaussian wave fronts[33] instead of the simplified plane-wave approximation used here. This difference between real and approximated wave fronts may be less for the measurements made with the more highly focused beams, which would account for the better fit between theory and experiment for this case.

VII. DISCUSSION AND CONCLUSIONS

The preceding sections described the results of an extensive investigation of $Nd_xLa_{1-x}P_5O_{14}$ crystals using four-wave-mixing spectroscopy. The most significant results of this work can be summarized as follows. Under appropriate experimental conditions, both population and thermal gratings can be established. The nonlinear interaction between the laser fields in the material which creates these gratings cannot be described by a simple two-level—system susceptibility model. Spatial exciton migration contributes to the destruction of the population grating, and characteristics of the exciton dynamics can produce different grating decay patterns. The energy migration can be enhanced through vibronic processes which populate the upper crystal-field component of the metastable state and through excitation processes which selectively excite higher-concentration subsets of ions within the inhomogeneous spectral profile. The dominant scattering mechanism which limits the exciton mean free path appears to be scattering from defects and boundaries in the crystals.

The theory of four-wave-mixing interactions in solids is still in the process of being developed. The multiple-energy-level system treated here allows the inclusion of excited-state absorption and dispersion effects not present in a simple two-level system. Although there is no *a priori* justification of using a linear combination of susceptibilities as done in Sec. VI, this is the simplest way of treating a multilevel system and is meant only to be a first approximation in the development of this type of model. The theory predicts a strong deviation from the quadratic dependence of scattering efficiency on pump power predicted by a two-level—system model, which is consistent with the experimental results. Future development of this model should involve more sophisticated methods for treating the susceptibility of a multilevel system, the effects of Gaussian wave fronts,[33] and the effects of beam depletion. Some progress in the latter area has been reported recently.[36]

Vibronic excitation has been employed in previous investigations of energy transfer and electron-phonon interactions of ions in crystals.[37] The results described in Sec. IV show the potential usefulness of this technique for studying the role played by phonons in the processes contributing to the establishment and decay of the population grating in four-wave mixing. The increase in the population of the upper crystal-field component of the metastable state, due to the selective generation of phonons whose energy is identical with that of the crystal-field splitting, is similar to the observations reported by Rives *et al.*[38] in other types of experiments. Since the resonant transition in this case actually involves several overlapping crystal-field components, it might be expected that several vibronic enhancement peaks should be seen. For example, these should appear near 5735 and 5748 Å. Although there appears to be some increase in D in the former location, both of these wavelengths are in the region where direct absorption begins to occur. It is not possible to develop a greater understanding of the vibronic processes without having available more detailed information concerning the phonon properties of the host crystal.

It is important to define the term coherence since it is commonly used in different ways to describe energy transfer in solids.[1–3] Some authors reserve the term coherence for describing the case where the ion-ion interaction is so strong that the energy transfer must be described by a spreading wave packet using Schrödinger's equation. Others have used the term to describe the case where an exciton moves as a quasiparticle with a given momentum so that it travels over many lattice spacings, maintaining its phase memory before scattering occurs. If numerous scattering events occur within the lifetime of the exciton, this can still be described by a diffusion equation. The use of the term coherence in Sec. V is associated with this type of long—mean-free-path exciton motion.

The observation of experimental results which may be interpreted in terms of partially coherent exciton migration reported here is extremely important since it can provide an opportunity to experimentally study the characteristics of this type of quasiparticle motion. Theoretical models of this type of energy transfer have been developed previously without any possibility of experimental verification. The work of Kenkre[25,26] provides the theoretical model most closely describing the experimental situation of this study. However, approximations made in Kenkre's

model needed to obtain a tractable expression for comparing with experimental results, make it impossible to obtain an exact fit to the data as shown in Sec. V. It appears to be difficult to modify Kenkre's generalized master-equation approach to include the possibility of time-dependent interaction parameters, and thus it may be better in this case to start from the stochastic Liouville equation as done by other workers.[39,40] This is an important problem for future theoretical work.

The ion-ion—interaction rate in neodymium pentaphosphate has been estimated in different ways and ranges from 2.4×10^7 s^{-1}, obtained from nearest-neighbor dipole-dipole interaction,[41] to 9.0×10^8 s^{-1}, obtained from a spreading—wave-packet calculation.[42] The experimental value for j obtained in this work is close to the former estimate. The value for the exciton scattering rate cannot be determined as specifically from the experimental data as discussed in Sec. V. The range of possible values of α between 10^4 and 3×10^6 s^{-1} is consistent with the dephasing rate of 5×10^4 s^{-1} measured by coherent transient spectroscopy methods[11] on the similar stoichiometric rare-earth crystal EuP_5O_{14}. The observation that acoustic phonons are not active in scattering the migrating exciton is not surprising since the wavelengths of acoustic phonons are much greater than the nearest-neighbor ion separations. This means that this type of phonon will modulate the energy levels of ions in neighboring sites simultaneously and will not be effective in causing scattering as the energy-transfer interaction occurs between these ions. The determination of the exact mechanism causing the exciton scattering is an important area for future research. The fact that the acoustic phonons are not effective in scattering excitons does not imply that they do not effect the overall characteristics of the exciton dynamics of the system. It is obvious from the results that the presence of phonons can effect the ion-ion—interaction rate in several ways.

The diffusion length of the excitons given by $L=\sqrt{2D\tau}$ is found from these results to be of the order of 1 μm, which is a significant fraction of the peak-to-valley grating spacing as required for transient-grating experiments. The exciton mean free path given by $\Lambda=v_g/\alpha$ ranges from about 1 μm to values over 2 orders of magnitude smaller than this, depending of the value used for α. Thus the lower-limit value for α predicts the excitons moving with no scattering during their lifetimes, i.e., completely coherent motion, whereas using the upper limit for α predicts hundreds of scattering events during the migration of the excitons. The overall results of this investigation are more consistent with the latter type of exciton migration.

The general consistency of the experimental results and the theoretical model presented here does not give conclusive proof that the observed oscillatory grating decay pattern is produced by partially coherent exciton migration. It is important to emphasize that these oscillations were observed only under very special experimental conditions and that these conditions are consistent with the required conditions of the Wong-Kenkre theory for predicting this type of decay pattern. Under different experimental conditions neither the Wong-Kenkre theory nor other theories[20,39,40] predict the appearance of oscillations and none are observed. It is possible that some other type of physical process is responsible for these results. However, no other mechanism consistent with the experimental results has been discussed in the literature, and therefore this question can only be answered through further experimental investigations.

The four-wave-mixing transient-grating spectroscopy technique employed here monitors the spatial migration of energy. The results show this energy migration to be very efficient and essentially independent of temperature. Other techniques monitoring the spectral diffusion of energy show these processes to be much less efficient and temperature dependent.[8–10] Techniques employing activator ions as traps can also detect spatial energy migration although the results may be difficult to interpret exactly due to the presence of trapping effects. Research of this type on rare-earth-doped neodymium pentaphosphate crystals has been interpreted in terms of fast diffusion of energy among the Nd^{3+} ions.[43,44] The coherent transient spectroscopy work mentioned earlier indicates that the exciton wave function in EuP_5O_{14} may be spread out over several lattice spacings, indicating strong resonant energy transfer. Other earlier studies of energy transfer in NdP_5O_{14} crystals resulted in conflicting conclusions concerning the extent of the energy migration.[45,46] Some of the apparent inconsistencies between early work and recent work may be due to the significant improvement in sample quality during this time interval.[13] Furthermore, different techniques may probe different types of physical processes. Spectral diffusion measurements may not be able to detect resonant ion-ion energy transfer in highly concentrated crystals under certain conditions. Thus it may be that transient-grating spectroscopy and site-selection spectroscopy are providing complementary information concerning the characteristic of this material instead of conflicting results. The interpretation of the results of the power dependence of D in terms of a power-broadening effect is consistent with the fact that this experimental technique is probing long-range resonant energy migration and is not sensitive to short-range spectral diffusion effects.

In conclusion, this work demonstrates the power of four-wave-mixing transient-grating spectroscopy in probing the details of spatial energy migration in highly concentrated solids. Along with the development of more detailed theoretical models discussed above, it is important to extend this type of experimental investigation to other types of materials. In addition, the work on NdP_5O_{14} should be extended to include even lower temperatures and to better define the transition from the high-mobility region of resonant excitation to the lower-mobility region of vibronic excitation.

ACKNOWLEDGMENTS

This work was supported by the U. S. Army Research Office, and National Science Foundation under Grant No. DMR-82-16551.

[1]V. M. Kenkre, in *Exciton Dynamics in Molecular Crystals and Aggregates,* edited by G. Hohler (Springer, Berlin, 1982), p. 1.
[2]C. B. Harris and D. S. Zwemer, Ann. Rev. Phys. Chem. 29, 473 (1978).
[3]R. Silbey, Ann. Rev. Phys. Chem. 27, 203 (1976).
[4]N. F. Mott, Adv. Phys. 16, 49 (1967).
[5]J. Koo, L. R. Walker, and S. Geschwind, Phys. Rev. Lett. 38, 858 (1977); S. Chu, H. M. Gibbs, S. L. McCall, and A. Passner, Phys. Rev. Lett. 45, 1715 (1980).
[6]K. Godzik and J. Jortner, J. Chem. Phys. 38, 227 (1979); Chem. Phys. Lett. 63, 3 (1979).
[7]G. Huber, in *Current Topics in Materials Science,* edited by E. Kaldis (North-Holland, Amsterdam, 1980), Vol. 4, p. 1.
[8]J. M. Flaherty and R. C. Powell, Phys. Rev. B 19, 32 (1979).
[9]R. C. Powell, D. P. Neikirk, J. M. Flaherty, and J. G. Gualtieri, J. Phys. Chem. Solids 41, 345 (1980).
[10]M. M. Broer, D. L. Huber, W. M. Yen, and W. K. Zwicker, Phys. Rev. Lett. 49, 394 (1982).
[11]R. M. Shelby and R. M. Macfarlane, Phys. Rev. Lett. 45, 1098 (1980).
[12]C. M. Lawson, R. C. Powell, and W. K. Zwicker, Phys. Rev. Lett. 46, 1020 (1981); Phys. Rev. B 26, 4836 (1982); J. K. Tyminski, R. C. Powell, and W. K. Zwicker, in *Lasers '82,* edited by R. C. Powell (STS, McLean, Virginia, 1983), p. 105. R. D. Plattner, W. W. Kruhler, W. K. Zwicker, T. Kovats, and S. R. Chinn, J. Cryst. Growth 49, 274 (1980).
[14]H. G. Danielmeyer and H. P. Weber, IEEE J. Quant. Electron. QE-8, 805 (1972).
[15]H. G. Danielmeyer, in *Festkörperprobleme,* edited by H. J. Queisser (Pergamon, New York, 1975), Vol. 15, p. 253.
[16]H. P. Weber, Opt. Quantum Electron. 7, 431 (1975).
[17]D. M. Pepper, Opt. Eng. 21, 156 (1982).
[18]J. K. Tyminski, Ph.D. dissertation, Oklahoma State University, 1983.
[19]H. Kogelnik, Bell System Tech. J. 48, 2909 (1969).
[20]M. D. Fayer, in *Spectroscopy and Excitation Dynamics of Condensed Molecular Systems,* edited by V. M. Agranovich and R. M. Hochstrasser (North-Holland, Amsterdam, 1983), p. 185; J. R. Salcedo, A. E. Siegman, D. D. Dlott, and M. D. Fayer, Phys. Rev. Lett. 41, 131 (1978).
[21]H. J. Eichler, J. Eichler, J. Knof, and Ch. Noack, Phys. Status Solidi A 52, 481 (1979).
[22]P. F. Liao, L. M. Humphrey, D. M. Bloom, and S. Geschwind, Phys. Rev. B 20, 4145 (1979).
[23]P. F. Liao and D. M. Bloom, Opt. Lett. 3, 4 (1978).
[24]D. S. Hamilton, D. Heiman, J. Feinberg, and R. W. Hellwarth, Opt. Lett. 4, 124 (1979).
[25]Y. M. Wong and V. M. Kenkre, Phys. Rev. B 22, 3072 (1980).
[26]V. M. Kenkre, Phys. Rev. B 18, 4064 (1978).
[27]V. M. Agranovich and M. D. Galanin, *Electronic Excitation Energy Transfer in Condensed Matter* (North-Holland, Amsterdam, 1982).
[28]V. M. Agranovich and Yu. V. Konobeev, Fiz. Tverd. Tela (Leningrad) 5, 1373 (1963) [Sov. Phys.—Solid State 5, 999 (1966)]; 6, 831 (1964) [6, 644 (1964)]; Phys. Status Solidi 27, 435 (1968); Opt. Spectrosc. 6, 155 (1959).
[29]A. Szabo and M. Kroll, Opt. Lett. 2, 10 (1978).
[30]H. Eichler and H. Stahl, J. Appl. Phys. 44, 3429 (1973); H. Eichler, G. Salje, and H. Stahl, *ibid.* 44, 5383 (1973).
[31]S. R. Chinn and W. K. Zwicker, J. Appl. Phys. 49, 5892 (1978).
[32]A. Yariv and D. M. Pepper, Opt. Lett. 1, 16 (1977).
[33]A. E. Seigman, J. Opt. Soc. Am. 67, 545 (1977).
[34]R. L. Abrams and R. C. Lind, Opt. Lett. 2, 94 (1978); 3, 205 (1978).
[35]*Optical Phase Conjugation,* edited by R. A. Fisher (Academic, New York, 1983).
[36]N. C. Kothari, M. Yoshizawa, and T. Kobayashi, Opt. Commun. 45, 211 (1983).
[37]F. Auzel, D. Meichenin, and J. C. Michel, J. Lumin. 18-19, 97 (1979); F. Auzel, J. Dexpert-Ghys, and C. Gautier, J. Lumin. 27, 1 (1982).
[38]J. E. Rives and R. S. Meltzer, Phys. Rev. B 16, 1808 (1977); G. D. Dixon, J. E. Rives, and R. S. Meltzer, in *Lasers '82,* Ref. 12.
[39]P. Reineker and R. Kuhne, Phys. Rev. B 21, 2448 (1980).
[40]J. L. Skinner, H. C. Anderson, and M. D. Fayer, Phys. Rev. A 24, 1994 (1981).
[41]P. F. Liao, H. P. Weber, and B. C. Torfield, Solid State Commun. 16, 881 (1975).
[42]A. Lempicki, Opt. Commun. 23, 376 (1977).
[43]W. Lenth, G. Huber, and D. Fay, Phys. Rev. B 23, 3877 (1981); D. Fay, G. Huber, and W. Lenth, Opt. Commun. 28, 117 (1979).
[44]G. Huber, J. P. Jeser, W. W. Kruhler, and H. G. Danielmeyer, IEEE J. Quantum Electron. QE-10, 766 (1974).
[45]H. P. Weber and P. F. Liao, J. Opt. Soc. Am. 64, 1337 (1974); P. F. Liao, H. P. Weber, and B. C. Tofield, Solid State Commun. 16, 881 (1973).
[46]S. Singh, D. C. Miller, J. R. Potopowicz, and L. K. Shick, J. Appl. Phys. 46, 1191 (1975).